

# Phase Measurement Using DIC Microscopy\*

Krisztian Koos<sup>a</sup>, Begüm Peksel<sup>a</sup>, and Lóránd Kelemen<sup>a</sup>

## Abstract

The development of fluorescent probes and proteins has helped make light microscopy more popular by allowing the visualization of specific subcellular components, location and dynamics of biomolecules. However, it is not always feasible to label the cells as it may be phototoxic or perturb their functionalities. Label-free microscopy techniques allow us to work with live cells without perturbation and to evaluate morphological differences, which in turn can provide useful information for high-throughput assays. In this study, we use one of the most popular label-free techniques called differential interference contrast (DIC) microscopy to estimate the phase of cells and other nearly transparent objects and instantly estimate their height. DIC images provide detailed information about the optical path length (OPL) differences in the sample and they are visually similar to a gradient image. Our previous DIC reconstruction algorithm outputs an image where the values are proportional to the OPL (or implicitly the phase) of the sample. Although the reconstructed images are capable of describing cellular morphology and to a certain extent turn DIC into a quantitative technique, the actual OPL has to be computed from the input DIC image and the microscope calibration settings. Here we propose a computational method to measure the phase and approximate height of cells after microscope calibration, assuming a linear formation model. After a calibration step the phase of further samples can be determined when the refractive indices of the sample and the surrounding medium is known. The precision of the method is demonstrated on reconstructing the thickness of known objects and real cellular samples.

**Keywords:** DIC microscopy, image processing, phase imaging, quantitative phase microscopy

## 1 Introduction

In the area of optical microscopy, the simplest technique is brightfield microscopy, which was invented by Anton van Leeuwenhoek [30] in the 17th century as an

---

\*This study was supported by the Hungarian National Brain Research Programme (MTA-SE-NAP B-BIOMAG), the CONCERT-Japan Photonic Manufacturing Joint Call, and by OTKA NN-114692.

<sup>a</sup>Hungarian Academy of Sciences, Biological Research Centre, E-mail: {koos.krisztian,begum.peksel,kelemen.lorand}@brc.mta.hu

improved version of the modern microscope developed by Robert Hooke [10]. Phase contrast microscopy was proposed in the early 1930s by Fritz Zernike, who was awarded the Nobel Prize in Physics in 1953 for his invention [25]. Phase contrast microscopy is interference-based and allows the study of the internal structure of living cells. Two years later, in 1955, Georges Nomarski established the theoretical basis for differential interference contrast (DIC) microscopy [24], which allows us to obtain information about the optical path length of the sample and shows features that are invisible in a brightfield microscope.

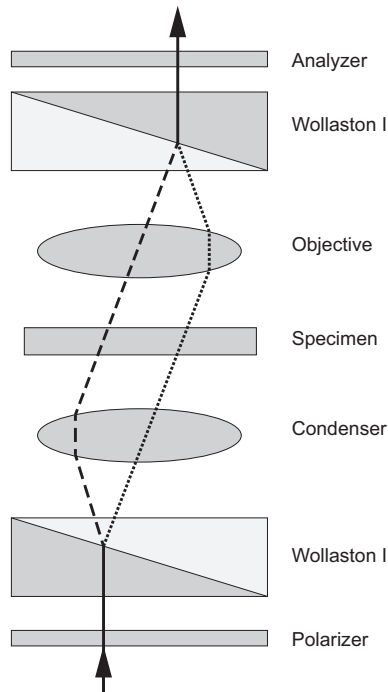


Figure 1: Setup of a DIC microscope. The arrows show the direction of the light. The dashed and dotted lines indicate the two mutually perpendicularly polarized light rays. The image formation starts as a light ray enters a polarizer that creates plane polarized light. A Wollaston prism splits the light into two perpendicularly polarized light rays, which are focused on the specimen by the condenser lens. These two light rays pass the sample by a minute shear. Materials with different refractive indices and the specimen's thickness generate a phase shift between the light rays. Next, a second lens, i.e. the objective, transmits the light to another Wollaston prism that recombines them. Finally, the analyzer creates plane polarized light perpendicular to the light of the first polarizer. The two light rays interfere at this point and generate a contrast image.

Brightfield, phase contrast and DIC microscopy are a set of label-free techniques. Such techniques cannot be used to selectively visualize subcellular components, processes, or the localization of proteins, and this stimulated a demand for new methods in microscopy. In 1994 a discovery brought fluorescence to the forefront [32]. Proteins can be stained by fluorescent substances which show their localization inside the cells. Fluorescent images are quantitative, thus they may be analyzed by a suitable software. In contrast, label-free techniques, especially phase contrast and DIC, are qualitative methods. Although these images are easy to interpret with a human eye, conventional algorithms cannot be applied when it comes to image processing. However, DIC has some advantages over fluorescent microscopy: namely, cells can be observed without staining, so the technique is non-phototoxic and there is no need to fix the sample - in contrast to numerous fluorescent staining protocols. Phototoxicity often occurs upon the exposure of fluorescently labeled cells to light. Fluorescent molecules excited by light react with molecular oxygen that can damage subcellular components or the entire cell. Thus DIC allows live cell analysis in a physiologically more relevant way.

Over time, many techniques have been developed that convert a qualitative label-free microscopy into a quantitative technique. These techniques are collectively called Quantitative Phase Microscopy (QPM) [7, 18, 19]. An example is diffraction phase microscopy (DPM) [4, 12] which shifts the light all over the image and after a reconstruction step the phase differences are visible with high precision. However, the technique requires a special device and it is not widely used. DIC is a cost-effective solution and it should be turned into a quantitative technique. Determining the image formation model [11, 20, 21, 22, 28] of DIC is important in developing a correct reconstruction algorithm. The image in a DIC microscope is formed by using plane polarized light, separated by a Wollaston or Nomarski prism. The light rays are separated at a subpixel distance. The sample as a phase object shifts the light rays, which are then recombined and the very small differences produce a contrast image. The schematic DIC setup is illustrated in Figure 1 and Figure 2 shows an example DIC image.

Many mathematical models have been developed for the DIC image formation, some of which are listed below. The light in a DIC system is partially coherent and so it is not well defined. The level of coherence may vary inside the system which should also be taken into account. Moreover, the samples are usually not purely phase objects, hence the image is formed by both the phase difference and amplitude change. Theoretical developments were also carried out to reconstruct the amplitude along with the phase using the Transport of Intensity theorem [16, 33, 34]. DIC was converted into a quantitative technique earlier by modifying it to Phase-shifting DIC (PS-DIC) [6, 13]. PS-DIC utilizes an additional part that is able to introduce a constant phase shift to the light rays. PS-DIC virtually has the effect of rotating the sample - in other words, it changes the shear direction of the microscope, thus allowing edges otherwise invisible to be observed by the technique. Reconstructing the scene from multiple images using a linear model provides a result with a 15% error [3, 27]. However, physically rotating the sample is not possible after we have inserted the slide and using more images for a single

scene reconstruction increases the computational complexity and acquisition time. Attempts were made to reconstruct the true phase from single images using different reconstruction algorithms [31], but the results have not been validated. In this paper, we present a method that reliably converts DIC into a quantitative technique using just a single image.

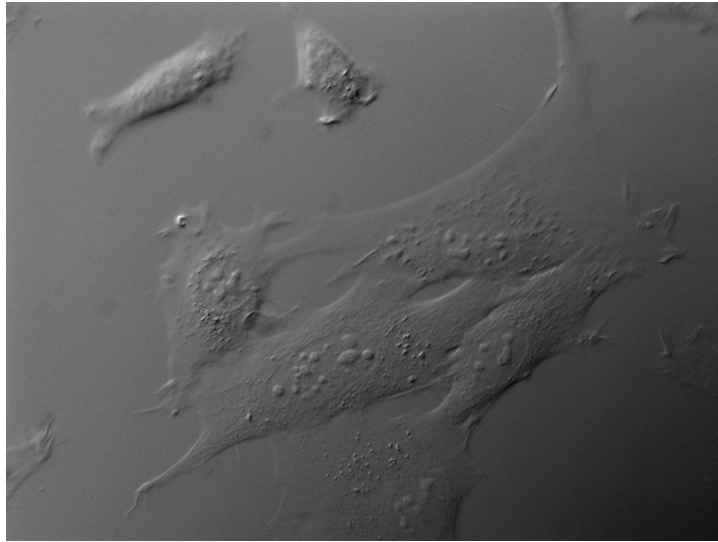


Figure 2: An example DIC image of cells. A well-configured DIC microscope provides sharp and detailed images. A trained eye can easily see the cells and the subcellular components, e.g. nucleoli. However, it is not straightforward to process, e.g. segment DIC images, without performing some transformation.

## 2 Methods

### 2.1 DIC reconstruction task

Images are treated as real-valued intensity functions parameterized by the image coordinates. Image coordinates and the domain of the intensity function are denoted by  $x$ ,  $y$  and  $\Omega$  ( $\{x, y\} \in \Omega$ ). Local integration domains are small square windows  $W$  around the image points. In these local windows, parameters  $\xi$  and  $\eta$  are used to define the local coordinates aligned with the  $x$  and  $y$  coordinates of the image. The symmetric domain of the local windows have sizes  $\delta$  in each direction:  $\xi, \eta \in W$ ,  $W = [-\delta, \delta] \times [-\delta, \delta]$ .  $d\Omega = dx dy$  and  $dW = d\xi d\eta$  represent the infinitesimal area elements of the integrals in the image and in the local domains, respectively. Partial derivatives of  $n$ th order are denoted by  $\partial_x^n$ ,  $\partial_y^n$ , and for  $n = 1$  we use the notation  $\partial_x$ ,  $\partial_y$ .

The aim of the DIC reconstruction is to create the primary image  $I(x, y)$  based on the known DIC image  $G(x, y)$ , where parameters  $x$  and  $y$  are the pixel coordinates of the images.

DIC images are often treated as directional intensity difference images. This supposes that the image formation model is linear, which was previously shown to be highly correlated to advanced image formation models [15] in typical cases where the amount of diffraction is low. The direction is defined by the imaging device and given a priori. Mathematically, the reconstruction based on this simple interpretation can be formalized in the following way: we wish to retrieve the primary image  $I$  from its known directional difference image  $G$ . The two images are related by the equation

$$G(x) = I(x+d) - I(x-d), \quad (1)$$

where  $x$  is the parameter along the predefined direction and device parameter  $d$  is proportional to the phase shift difference between two light beams (reference beam and measuring beam). The difference on the right-hand side can also be represented by the integral  $\int_{x-d}^{x+d} I'(\zeta) d\zeta$ , where  $I'$  is the directional derivative of the primary image. The direct generalization of this integral is  $\int_{x-d}^{x+d} K(\zeta-x) I'(\zeta) d\zeta = \int_{x-d}^{x+d} K(\zeta) I'(x+\zeta) d\zeta$  with some appropriately chosen finite kernel  $K$ . A further generalization to two dimensions can be defined by using the partial derivatives of the local integral

$$\hat{I}(x, y) = \iint_W K(\xi, \eta) I(x+\xi, y+\eta) dW, \quad (2)$$

with a two-dimensional finite kernel  $K$  such that

$$G = \mathbf{u} \cdot \nabla \hat{I}, \quad (3)$$

where  $\mathbf{u} = [u \ v]^T$  is a unit vector ( $u^2 + v^2 = 1$ ) in the shear direction determined by the imaging device. Note that image  $\hat{I}$  is the convolved version of  $I$  and the integral (2) is a parametric integral w.r.t. the image coordinates  $x$  and  $y$ .

## 2.2 Reconstruction using a variational framework

We use a variational framework based on (3) to reconstruct DIC images. In a variational framework [5, 23, 26], we have to define an energy function that usually consists of a data term and one (or more) regularization term:

$$E = E_{data} + \lambda E_{reg}. \quad (4)$$

The local integral in (2) can be used as a data term in an energy functional expressing that the proper reconstruction of the primary image satisfies (3), for example

$$E_{data} \doteq \frac{1}{2} \iint_{\Omega} [\mathbf{u} \cdot \nabla \hat{I} - (G - c)]^2 d\Omega \doteq \frac{1}{2} \iint_{\Omega} S^2 d\Omega$$

$$S = \iint_{\xi, \eta} K (u \partial_x I + v \partial_y I) d\xi d\eta - (G - c). \quad (5)$$

Note that any arbitrary constant  $c$  can be added to the DIC image  $G$  without affecting the solution. The spatial regularization term ensures that we have locally smooth regions where  $G$  is smooth (i.e. there are no edges in the original image) and it has no effect on high image gradients. For this latter term, we use the total variation (TV) [29], which has the form

$$|\nabla I| = \sqrt{(\partial_x I)^2 + (\partial_y I)^2}. \quad (6)$$

To apply the gradient descent algorithm, the Euler-Lagrangian (EL) of the two terms in (5) and (6) have to be calculated. The complete derivation of the EL equations can be found in [14] and [15], but here we only describe and explain the final equations. The EL equation of the data term is very complex because of the local integrals introduced by the kernel function. Instead, we calculate the Taylor series of the perturbation function. Since the light ray pairs, separated by the DIC prism in the microscope setup, are at a subpixel distance from each other, we assume the perturbation function to be a piecewise analytic function, which is a requirement before replacing it by the Taylor series. In other words, the Taylor series is convergent around each image point, or at least in the domain of the local integration. In practice, we found that the first two terms provide sufficiently accurate results.

At this point, the gradient descent algorithm can already be applied iteratively. However, the intuition that the kernel function (or point spread function, PSF) has to encode some directional derivative effect is not straightforward here. Currently, the shadow-cast effect is described by the  $u \cdot \nabla$  operator and although  $K$  can be chosen arbitrarily for the equation to remain true, an obvious choice would be a rotationally symmetric function  $K_R$ . With a parameter transformation, the calculation of derivatives can be moved from the image to the kernel, which allows the use of an approximation of the DIC PSF. This way, the second order derivatives of the PSF function have to be calculated and then used as a convolution kernel, which is computationally more expensive than calculating image derivatives and convolving with a single kernel. The rotationally symmetric function  $K_R$  further reduces the 'bilinear' equation to the following 'piecewise constant' approximation:

$$0 = \mathbf{u} \cdot \nabla G - \iint_{\xi, \eta} K_R \mathbf{u} \cdot \nabla \nabla I \cdot \mathbf{u} d\xi d\eta. \quad (7)$$

The EL equation of the TV term has the following form [1, 29]:

$$0 = \frac{\delta}{\delta x} \left( \frac{\delta_x I}{|\nabla I|} \right) + \frac{\delta}{\delta y} \left( \frac{\delta_y I}{|\nabla I|} \right) \quad (8)$$

It is known that TV can remove noise, while preserving sharp signals.

### 2.3 Other reconstruction algorithms

In our recent paper [15], we described and compared the most relevant DIC reconstruction algorithms. These algorithms can be organized into groups based on their computational principles.

One major group is based on inverse filtering. Inverse filtering algorithms describe the reconstruction problem as a division in Fourier space. Frequency space calculations are very fast and these algorithms are direct, i.e. they provide a solution in one step. The Hilbert transform [2, 9] is considered to be the first algorithm that was used to reconstruct DIC images. Another widely used algorithm is Wiener filtering [9, 31], which avoids division by values close to zero. A third approach from this group is based on pure Fourier space operations with additional regularization terms [35] (referred to as Yin). Regularization terms in frequency space also help to avoid division by zero and they help to remove artefacts from the image and provide a smooth reconstruction.

A second group of algorithms is based on linear programming. The reconstruction problem is formed as a linear equation system, which is then solved by some algorithm. The image formation model is coded in a transfer matrix and the regularization terms, i.e. smoothness or sparsity are also expressed in matrix forms. Two linear equation system solvers have been proposed [17] to solve the DIC reconstruction problem, namely the sparseness-enhanced multiplicative update (SEMU) and a second order cone program (SOCP).

The third group of DIC reconstruction algorithms use a variational framework. The algorithm presented in Section 2.2 falls in this group (referred to as Koos), while another energy minimization method was presented in [8] (Feineigle). The Feineigle algorithm considers image formation as a directional derivation and does not incorporate the PSF of the microscope system, and the energy function is minimized based on its Eulerian equation.

Figure 3 shows 3 sample image series to compare the above mentioned algorithms. The input simulated DIC images are computed from the ground truth images by convolving them with a PSF, assuming a linear image formation model, which is known to be very close to the correct image formation model [15]. The difference in the output quality of the algorithms is visible. Better performing algorithms produce correct, visually indistinguishable results from the ground truths. The reconstructions of weaker algorithms, usually the inverse filtering based ones, are either blurred or only the outlines of the objects are correct. Furthermore, the algorithms often fail to reconstruct small changes, e.g. gradients in the ground truth, which is a necessity when it comes to cells. This effect is shown in the third,

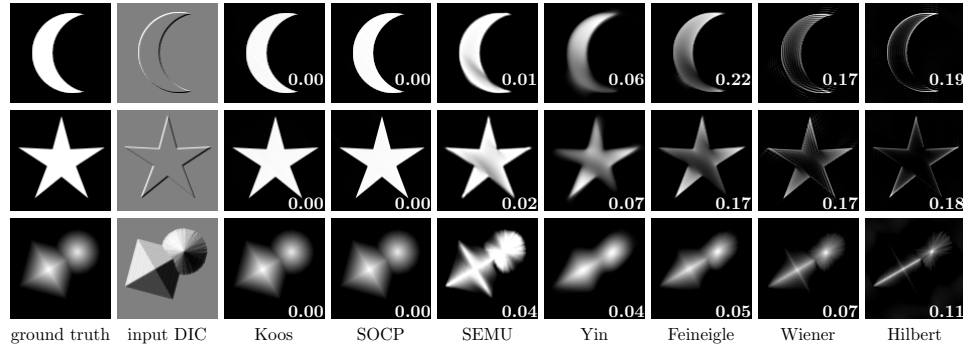


Figure 3: A comparison of DIC reconstruction algorithms. The first column contains ground truth images that the algorithms attempt to reconstruct. The images in the second column are the simulated DIC images of the ground truths, which are the input data of the algorithms. The shear direction in the simulation is -45 degrees, which is passed as prior knowledge to the algorithms. The following columns contain result images in decreasing order based on the algorithms' quality measured by the averaged mean squared error (MSE) taken from 20 images and their rotations. The values in the reconstructed images are the MSE values.

grayscale example in Figure 3. Since the variational framework presented in Section 2.2 performed the best in our comparison study, we decided to apply it in all subsequent computations.

## 2.4 An algorithm for phase and height reconstruction

In this section, we describe an algorithm used to measure the phase and height of unknown objects. The algorithm starts with a calibration process that aims to determine the relation between the values in the reconstructed images and the phase of the examined objects. The assumption of a linear image formation model has to be made, because it is already required by the reconstruction algorithms. The linear image formation model (in terms of phase) means that the sample is a phase object and does not absorb light, i.e. the amplitude of light does not change. Cells only absorb about 10% of light and in practice they are considered as phase objects.

As a first step, the microscope settings have to be fixed: the illumination and exposure time have to be set to a constant value, and a bandpass filter should be used if available. Using filters makes it easier to calculate a weighted average of wavelengths or a narrower range can be used later to calculate the phase. Furthermore, any other microscope specific parameters should be fixed that affect the image acquisition, i.e. image histogram operations should be disabled. Most microscope software can automatically determine these parameters, but only for the

sample being observed. The final settings can be based on the automatic values but they should be set manually so that they are suitable for both the calibration objects and the further samples.

The next step is the phase calibration. Images should be taken of some calibration samples. Calibration objects usually have simple shapes and are homogeneous. Moreover, the refractive index of both the sample and the surrounding medium has to be known in advance. After reconstructing the DIC images of the calibration samples, the reconstructed object values are fit to the theoretical phase profile. Now the function that maps the reconstructed values to phase values can be calculated. This function can be used later (without altering the microscope settings) to determining the phase of unknown objects, but with known refractive indices. If the objects are not homogeneous, an averaged refractive index value can be used to get an approximation, as will be shown later in Section 3.2.

To perform the phase calibration, we used polystyrene microbeads of diameter  $d = 9\mu\text{m}$  (Polybead, Polysciences, Warrington, PA, USA). The refractive index of the beads is  $n_{bead} = 1.595$  and  $n_{oil} = 1.515$  for the oil (type DF, Cargille, Cedar Grove, NJ, USA) in which they are immersed. We used an Olympus IF550 bandpass filter for our tests which has an average weighted wavelength  $\lambda$  of about 550 nm. This  $\lambda$  value was then used to calculate the theoretical phase profile of the beads. The following equation gives the phase difference between the surrounding medium and the center of the bead:

$$\varphi = \frac{2\pi}{\lambda} \Delta n d, \quad (9)$$

where  $\Delta n = n_{bead} - n_{oil}$  in this case. Figure 2.4 shows an example DIC and reconstructed image of a microbead, and the averaged data fit to the theoretical phase profile. The data was normalized to the theoretical profile, which is a reliable method in the case of spheres, because the phase distribution is not uniform. The two line plots highly correlate. The flat-top behaviour of the measured data is attributed to the slight smoothing effect of the TV term, which preserves high jumps and flattens small differences. Based on the scales shown for the two  $y$  axes, a unit change in pixel intensity can be expressed as a phase change. This value can be used to express the phase of unknown objects. However, this approach does not consider diffraction effects due to the linearity of the model. If the phase difference is too high between the surrounding medium and the calibration object, diffraction causes artifacts in the DIC image which negatively affects the calibration.

The physical height of homogeneous samples can easily be calculated from the phase  $\varphi$ , if we know the wavelength  $\lambda$  and the refractive index difference  $\Delta n$  of the sample and the medium, using the following formula, which gives the height in nanometers:

$$h = \frac{\varphi \lambda}{2\pi \Delta n} \quad (10)$$

Algorithm 1 summarizes the process used for calibration and height estimation:

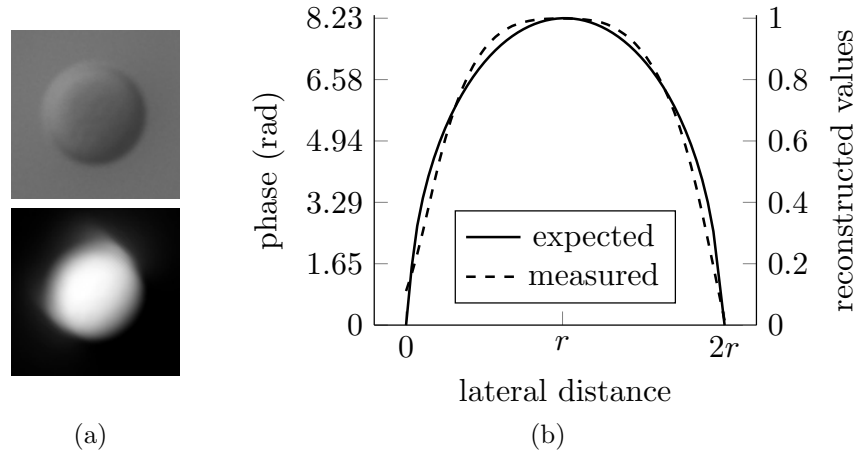


Figure 4: Phase calibration on microbeads. (a) Example DIC image of a microbead and its reconstruction. (b) Line profile of the expected phase distribution of a microbead and that of the reconstructions, where  $r$  is the radius of a microbead. The plot of the reconstruction was averaged over 16 beads after normalization, in 4 directions (horizontal, vertical and two diagonals) through the center of the beads.

---

**Algorithm 1** Measuring phase using DIC microscopy

---

- 1: Select a calibration sample with known dimensions and refractive index
  - 2: Perform a phase calibration
  - 3: Create images of the sample
  - 4: Reconstruct the DIC images
  - 5: Transform the reconstructed images to phase images
  - 6: Optionally convert phase to height
- 

If more than one type of sample needs to be imaged in one session, the calibration only has to be performed once, and from the second type the algorithm can be started from Step 3.

### 3 Results

In this section the algorithm described in Section 2.4 is validated on microbeads of different sizes. Then an example application is shown on images of cells, where the height of cells have also been calculated.

#### 3.1 Phase reconstruction on microbeads

To verify that the calibration is accurate, we created images of microbeads of different but known sizes under the same conditions, in the same medium. Then

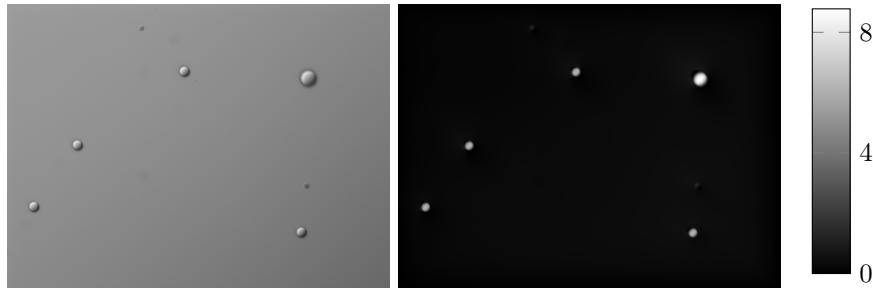


Figure 5: Example DIC image (left) of multiple sized microbeads and its reconstructed phase image (right) with a colormap. The phase was calculated after the phase calibration process (described in Section 2.4) had been performed.

the images were reconstructed and converted to phase images using the calibration function that was determined in the calibration process in Section 2.4. Finally, the observed peak values of the beads were compared to the theoretical peaks.

The diameters of the microbeads used for this test were 6 and 9  $\mu m$ . The microbeads, originally supplied in distilled water, were mixed and put on a coverslip. Then the coverslip was dried under heat to ensure that the microbeads were not drawn to each other when the water evaporated, thus reconstructed images should be more accurate. 7 DIC images were made of the coverslip and the peak values of 29 smaller and 7 bigger microbeads were determined. The average reconstructed phase for the 6  $\mu m$  beads were 5.81 rad, which is 0.33 rad more than the value that (9) gives. However, the variance in 6 and 9  $\mu m$  beads were only 0.12 and 0.14 rad, respectively. We think that the phase error between the different sized beads originates from the nonlinearity of the image formation and it is not a problem of the reconstruction process, because the variance is much less among the same sized beads. Furthermore, 0.33 rad converted to distance is about 180  $nm$ , which is fairly below the 10% size variance of the beads as given by the manufacturer. Figure 5 shows an example DIC image of microbeads and its reconstructed phase image.

### 3.2 Cell height measurement

To demonstrate the practical utility of phase reconstruction from DIC images, pictures of mouse embryonic fibroblast (MEF) cells were taken and reconstructed. Figure 6 contains example DIC images and their computed phase images. Rounded-up cells are brighter, while elongated (deformed) ones that have become attached to the bottom of the dish are mid-gray. Rounded-up cells are thought to have a similar volume to others, but they are taller. Since OPL is formed by the product of refractive index and thickness, taller cells appear brighter in the reconstructions. The nucleoli and other subcellular compartments appear as regions which demonstrates the resolution capability of the technique. Since (10) is linear, in the case of cells this transformation usually does not reflect the true height value. Although

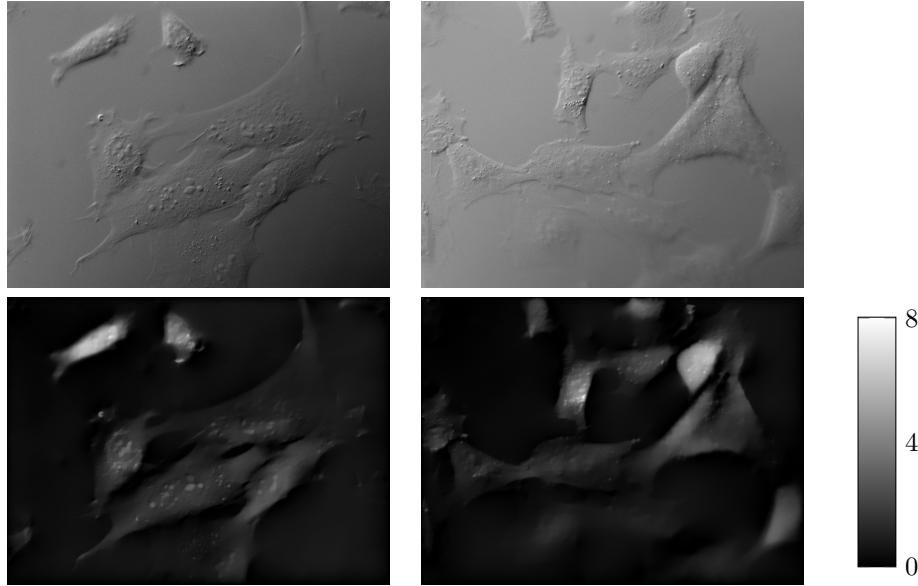


Figure 6: Example DIC images of MEF cells and their reconstructed phase images. The colorbar is in radians. The phases were calculated after the calibration process. Rounded-up cells are taller, hence appear brighter in the reconstructed images. The nucleoli and other compartments of the cells are clearly visible.

the nucleoli in Figure 6 have higher OPL, this is due to their higher refractive index and the cell height being smooth. If height information of cells is required, some statistical phase value (e.g. mean or median) should be used in the calculation. Furthermore, note that in spite of the microbeads having similar radian values in Figure 6 to Figure 5, it does not imply that the cells are of similar size to the microbeads. The refractive index difference  $\Delta n$  has a different value in the two cases, which results in significantly different height values when (10) is applied. The calculated height is about  $10 \mu m$  and  $20 \mu m$ , respectively, for attached and rounded-up cells which is in the range of the physical cell size.

## 4 Discussion

In this paper, a computational method was described to measure the phase of near-transparent objects using DIC microscopy. The method is based on a calibration process using an object with known dimensions and refractive index. The DIC images are reconstructed using a variational framework. The reconstructed images are then converted to phase or height images. The process is described in a step-by-step fashion in Algorithm 1. The calculations were verified on microbeads of different sizes and applied on cell images. The technique has a precision of about one

third wavelength. Compared to other microscopy techniques that were mentioned in Section 1 (e.g. PS-DIC and DPM), our technique provides a simple and cost-effective solution, it does not require additional microscope parts to be installed, and it reliably restores the phase information using just a single image.

## References

- [1] Alvarez, L., Lions, P.L., and Morel, J.M. Image selective smoothing and edge detection by nonlinear diffusion. II. *SIAM Journal on numerical analysis*, 29(3):845–866, 1992.
- [2] Arnison, M.R., Cogswell, C.J., Smith, N.I., Fekete, P.W., and Larkin, K.G. Using the Hilbert transform for 3D visualization of differential interference contrast microscope images. *Journal of microscopy*, 199(1):79–84, 2000.
- [3] Arnison, M.R., Larkin, K.G., Sheppard, C.J., Smith, N.I., and Cogswell, C.J. Linear phase imaging using differential interference contrast microscopy. *Journal of microscopy*, 214(1):7–12, 2004.
- [4] Bhaduri, B., Edwards, C., Pham, H., Zhou, R., Nguyen, T.H., Goddard, L.L., and Popescu, G. Diffraction phase microscopy: principles and applications in materials and life sciences. *Advances in Optics and Photonics*, 6(1):57–119, 2014.
- [5] Chan, T.F. and Vese, L. Active contours without edges. *IEEE transactions on Image processing*, 10(2):266–277, 2001.
- [6] Cogswell, C.J., Smith, N.I., Larkin, K.G., and Hariharan, P. Quantitative DIC microscopy using a geometric phase shifter. In *BiOS'97, Part of Photonics West*, pages 72–81. International Society for Optics and Photonics, 1997.
- [7] Cuche, E., Marquet, P., and Depeursinge, C. Simultaneous amplitude-contrast and quantitative phase-contrast microscopy by numerical reconstruction of Fresnel off-axis holograms. *Applied optics*, 38(34):6994–7001, 1999.
- [8] Feineigle, P.A., Witkin, A.P., and Stonick, V.L. Processing of 3D DIC microscopy images for data visualization. In *Acoustics, Speech, and Signal Processing*, volume 4, pages 2160–2163. IEEE, 1996.
- [9] Heise, B., Sonnleitner, A., and Klement, E.P. DIC image reconstruction on large cell scans. *Microscopy research and technique*, 66(6):312–320, 2005.
- [10] Hooke, R. *Micrographia: or some physiological descriptions of minute bodies made by magnifying glasses, with observations and inquiries thereupon*. Courier Corporation, 2003.
- [11] Kagalwala, F. and Kanade, T. Reconstructing specimens using DIC microscope images. *IEEE Transactions on Systems, Man, and Cybernetics, Part B (Cybernetics)*, 33(5):728–737, 2003.

- [12] Kim, T., Zhou, R., Goddard, L.L., and Popescu, G. Solving inverse scattering problems in biological samples by quantitative phase imaging. *Laser & Photonics Reviews*, 10(1):13–39, 2016.
- [13] King, S.V., Libertun, A.R., Preza, C., and Cogswell, C.J. Calibration of a phase-shifting DIC microscope for quantitative phase imaging. In *Proc. SPIE*, volume 6443, page 64430M, 2007.
- [14] Koos, K., Molnár, J., and Horvath, P. DIC Microscopy Image Reconstruction Using a Novel Variational Framework. In *Digital Image Computing: Techniques and Applications*, pages 1–7. IEEE, 2015.
- [15] Koos, K., Molnár, J., Kelemen, L., Tamás, G., and Horvath, P. DIC image reconstruction using an energy minimization framework to visualize optical path length distribution. *Scientific Reports*, 6, 2016.
- [16] Kou, S.S., Waller, L., Barbastathis, G., and Sheppard, C.J. Transport-of-intensity approach to differential interference contrast (TI-DIC) microscopy for quantitative phase imaging. *Optics letters*, 35(3):447–449, 2010.
- [17] Li, K. and Kanade, T. Nonnegative mixed-norm preconditioning for microscopy image segmentation. In *International Conference on Information Processing in Medical Imaging*, pages 362–373. Springer, 2009.
- [18] Mann, C., Yu, L., Lo, C.M., and Kim, M. High-resolution quantitative phase-contrast microscopy by digital holography. *Optics Express*, 13(22):8693–8698, 2005.
- [19] Marquet, P., Rappaz, B., Magistretti, P.J., Cuche, E., Emery, Y., Colomb, T., and Depeursinge, C. Digital holographic microscopy: a noninvasive contrast imaging technique allowing quantitative visualization of living cells with subwavelength axial accuracy. *Optics letters*, 30(5):468–470, 2005.
- [20] Mehta, S.B. and Oldenbourg, R. Image simulation for biological microscopy: microlith. *Biomedical optics express*, 5(6):1822–1838, 2014.
- [21] Mehta, S.B. and Sheppard, C.J. Partially coherent image formation in differential interference contrast (DIC) microscope. *Optics express*, 16(24):19462–19479, 2008.
- [22] Mehta, S.B. and Sheppard, C.J. Equivalent of the point spread function for partially coherent imaging. *Optica*, 2(8):736–739, 2015.
- [23] Mumford, D. and Shah, J. Optimal approximations by piecewise smooth functions and associated variational problems. *Comm. Pure Appl. Math.*, 42(5):577–685, 1989.
- [24] Murphy, D.B. and Davidson, M.W. *Differential interference contrast microscopy and modulation contrast microscopy. Fundamentals of Light Microscopy and Electronic Imaging, Second Edition p. 173-197.* 2001.

- [25] Murphy, D.B. and Davidson, M.W. *Phase contrast microscopy and darkfield microscopy. Fundamentals of Light Microscopy and Electronic Imaging, Second Edition p. 115-133.* 2001.
- [26] Osher, S. and Sethian, J.A. Fronts propagating with curvature-dependent speed: algorithms based on Hamilton-Jacobi formulations. *Journal of computational physics*, 79(1):12–49, 1988.
- [27] Preza, C., King, S.V., and Cogswell, C.J. Algorithms for extracting true phase from rotationally-diverse and phase-shifted DIC images. In *Biomedical Optics 2006*. International Society for Optics and Photonics, 2006.
- [28] Preza, C., Snyder, D.L., and Conchello, J.A. Theoretical development and experimental evaluation of imaging models for differential-interference-contrast microscopy. *JOSA A*, 16(9):2185–2199, 1999.
- [29] Rudin, L.I., Osher, S., and Fatemi, E. Nonlinear total variation based noise removal algorithms. *Phys. D*, 60:259–268, November 1992.
- [30] Schierbeek, A. *Measuring the invisible world: the life and works of Antoni van Leeuwenhoek*. Abelard-Schuman, 1959.
- [31] Van Munster, E.B., Van Vliet, L.J., and Aten, J.A. Reconstruction of optical pathlength distributions from images obtained by a wide-field differential interference contrast microscope. *Journal of Microscopy*, 188(2):149–157, 1997.
- [32] Vonesch, C., Aguet, F., Vonesch, J.L., and Unser, M. The colored revolution of bioimaging. *Signal processing magazine*, 23(3):20–31, 2006.
- [33] Waller, L., Tian, L., and Barbastathis, G. Transport of intensity phase-amplitude imaging with higher order intensity derivatives. *Optics express*, 18(12):12552–12561, 2010.
- [34] Waller, L., Tsang, M., Ponda, S., Yang, S.Y., and Barbastathis, G. Phase and amplitude imaging from noisy images by Kalman filtering. *Optics express*, 19(3):2805–2815, 2011.
- [35] Yin, Z. and Kanade, T. Restoring DIC microscopy images from multiple shear directions. In *Biennial International Conference on Information Processing in Medical Imaging*, pages 384–397. Springer, 2011.